Valence-shell photoabsorption spectra of C, Si, Ge, and Sn

F. Robicheaux and Chris H. Greene
Department of Physics and The Joint Institute for Laboratory Astrophysics, University of Colorado, Boulder, Colorado 80309-0440
(Received 13 November 1992)

We present the results of R-matrix calculations for the bound-state properties of the atoms in the carbon group for states with odd parity and $J=0-3$. The calculations were performed in LS coupling with the fine-structure interaction incorporated through an LS-jj frame transformation. We also present the photoionization cross section of the $ns^2np^2\,{}^3P_0$ ground state for each of the atoms for final-state energies between the two $ns^2np\,{}^2P^o_{J_c}$ spin-orbit split thresholds. We discuss some of the limitations of our method.

PACS number(s): 32.30.−r, 31.50.+w, 31.20.Di, 32.80.Fb

I. INTRODUCTION

There have been several experiments determining the bound-state Rydberg spectra of atoms in the carbon group for states with odd parity and $J=0-3$ [1–5]. The Rydberg series approach two ionic thresholds, $ns^2np\,{}^2P^o_{J_c}$, with $J_c=\frac{1}{2}$ and $\frac{3}{2}$. Other thresholds such as $nsnp^2$ and $ns^2(m+1)s$ have much higher energies, and the states attached to these thresholds do not enter the bound-state dynamics (except for a couple of notable exceptions). The Rydberg series interact with each other and can produce relatively complicated spectra. However, the spectra are amenable to a simple graphical description developed by Lu and Fano because there are only two relevant thresholds in our range of interest [6].

In this paper we describe a series of small-scale calculations which accurately reproduce the experimental energy levels of C, Si, Ge, and Sn. By studying several different types of atoms in one column of the Periodic Table, we would like to draw attention to the similarities (if any) in the Rydberg dynamics of chemically similar elements. There have also been extensive experiments on the carbon group of atoms that were interpreted in a semiempirical way using multichannel quantum-defect theory (MQDT) [1–5]. With their fitted parameters, Brown, Ginter, and co-workers [1–5] were able to reproduce a remarkable amount of data, identify regularities in the spectra, and draw attention to astonishing similarities of the Lu-Fano plots of the heavier atoms; these similarities are not apparent in the discrete absorption spectra. Our goal is to provide the first nearly *ab initio* description of these spectra; *ab initio* calculations can usually describe the energy dependence of dynamical parameters more correctly than semiempirical fits. Our goal is to obtain the MQDT parameters with moderate accuracy (at the percent level) over several eV and obtain a global understanding of the dynamics over a broad energy range; this goal complements efforts of those who strive for wave-number accuracy in the several lowest bound states. Thus, our motivation for studying these atoms parallel those for our studies of the halogen atoms [7].

All of the wave functions used in these calculations contain configuration interaction (CI). The ground state, the final state, and the target states are all computed using CI. The orbitals we use as a starting point are similar to those obtained by the Hartree-Fock method, but the final computation improves substantially over Hartree-Fock.

We utilize calculational and theoretical techniques identical to those of our previous studies [7], with one minor exception which is described in Sec. II B. We use the eigenchannel R-matrix approach [8] for the brute force part of the calculation and MQDT [9] to extend the wave functions to distances larger than the R-matrix box radius. The R-matrix calculation determines completely nonrelativistic LS-coupled short-range wave functions with the spin-orbit interaction incorporated in the MQDT part of the calculation by applying the LS to jj frame transformation [10].

The ground states of the carbon-group atoms are labeled $ns^2np^2\,{}^3P_0$ with $n=2$ for C, $n=3$ for Si, $n=4$ for Ge, and $n=5$ for Sn. In a photoabsorption process a p electron can be excited to an s or a d wave, and an s electron can be excited to a p wave. For this paper we will be focusing on the region below and between the $ns^2np\,{}^2P^o_{J_c}$ thresholds. In this energy range the important channels for photoabsorption are $ns^2np\,{}^2P\,\epsilon s$ and ϵd; also in this energy range are short-range resonances of the type $nsnp^3$ which perturb the $ns^2np\,\epsilon s$ and ϵd channels. These resonances cause the MQDT parameters to vary rapidly with energy for some of the LS symmetries. This paper is similar to Ref. [7(a)] in that we focus on the energy range where only the p electron can be excited.

II. THEORETICAL TECHNIQUES

We will describe in detail only one aspect of the methods we used to calculate the atomic properties since it is the only part different from our previous calculations [7].

A. Old methods

The major physical approximation concerns the Hamiltonian H, which does *not* refer to the full atomic system. H is strictly nonrelativistic, not even containing $\mathbf{l}_i\cdot\mathbf{s}_i$ interactions. Most importantly, H only represent the Ham-

iltonian of the valence shells [7,8]. The effect of the $Z-4$ inner-core electrons is approximated by a screened Coulomb potential plus a polarization potential. The valence-electron Hamiltonian in atomic units is

$$H=\sum_i H_V(\mathbf{p}_i,\mathbf{r}_i)+\sum_{\substack{i,j\\(i<j)}} 1/r_{ij} -2\sum_{\substack{i,j\\(i<j)}} P_1(\cos\theta_{ij})\sqrt{V_{\rm pol}(r_i)V_{\rm pol}(r_j)}\ , \quad (1)$$

where

$$\cos\theta_{ij}=\mathbf{r}_i\cdot\mathbf{r}_j/r_i r_j\ .$$

The computer code developed in Ref. [7] evaluates the angular part of the multielectron $1/r_{ij}$ matrix elements by summing products of 6-j coefficients. The one-electron Hamiltonian contains the interaction of the valence electron with the nucleus and the inner-core electrons and has the form

$$H_V(\mathbf{p},\mathbf{r})=p^2/2+V =p^2/2-(4+\{Z-4\}\exp\{-\alpha_1^l r\} +\alpha_2^l r\exp\{-\alpha_3^l r\})/r+V_{\rm pol}(r)\ . \quad (2)$$

Here

$$V_{\rm pol}=-\alpha_d(1-\exp\{-(r/r_c)^3\})^2/2r^4$$

represents the interaction of an outer electron with the inner core due to its dipole polarizability. We use the values of Ref. [11] for the dipole polarizability, α_d of the inner core for atoms of the carbon group; they are 0.008 92 for C, 0.1624 for Si, 0.7628 for Ge, and 2.264 for Sn. The parameters α_i^l and r_c are fitted to optimize agreement between the calculated energy levels of H_V and the experimental levels of the 3+ ion. We list our values for α_i^l and r_c in Table I. Unfortunately, the *nd* ionic levels of Ge and Sn are perturbed by a core excitation, and the number of levels to be fitted is minimal for these atoms, which may have introduced unacceptable errors in the α_i^l.

We use the streamlined formulation of the eigenchannel R-matrix procedure [8(a)] to find a variational estimate of the logarithmic derivative of the wave function at a given energy normal to the surface of the R-matrix volume. We define the R-matrix volume by $r_i\le r_c$ (i.e., all electrons confined to radii less than r_c), with r_c being 15 a.u. for the calculations reported here. The logarithmic derivative together with the value of the wave function at the surface completely determines the wave function everywhere outside of the R-matrix volume. The wave function outside can be written in the form [9]

$$\psi_i=\mathcal{A}\sum_j \Phi_j^{(LS)}(\Omega)[f_j(r)\delta_{ji}-g_j(r)K_{ji}^{(LS)}]\ , \quad (3)$$

where $\mathcal{A}$ is the antisymmetrization operator (which has no practical effect at $r>r_c$ since the outermost electron no longer overlaps the core electrons), $\Phi_j^{(LS)}(\Omega)$ represents the target function and the LS coupling of the target's angular momenta with that of the outer electron to give L and S, $f_j(r)$ is the radial Coulomb function [9] for channel j that is regular at the origin, $g_j(r)$ is the radial Coulomb function [9] for channel j that is irregular at the origin and oscillates 90° out of phase with respect to $f_j(r)$, and $\mathbf{K}^{(LS)}$ is the short-range reaction matrix. Open and closed channels are included in Eq. (3); thus, the ψ_i contain terms which are exponentially diverging at $r\to\infty$. The reaction matrix in Eq. (3) has the superscript LS to denote that it depends on the total spin and orbital angular momenta. The reduced dipole matrix elements connecting the initial state to each of the independent wave functions,

$$d_i=\langle\psi_i\|D\|\Psi_0\rangle\ , \quad (4)$$

are the only other short-range dynamical parameters needed to obtain the photoionization cross sections and oscillator strengths.

When the outer electrons leaves the atom, the rate of phase accumulation at large distances (and even whether it is bound or escapes to infinity) depends crucially on the

TABLE I. Parameters for the semiempirical potential for the valence electrons.

Atom	l	α_1^l	α_2^l	α_3^l	r_c (a.u.)
C	0–4	6.758 75	7.274 85	9.230 57	0.4
Si	0	5.280 51	8.759 03	3.598 75	0.4
	1	5.363 26	8.928 72	3.503 32	0.4
	2–4	5.031 25	8.847 00	4.329 46	0.4
Ge	0	4.831 39	8.755 88	3.084 73	0.4
	1	4.980 04	8.475 18	2.928 29	0.4
	2–4	4.914 06	9.029 35	3.206 25	0.4
Sn	0	5.463 33	10.486 64	2.303 93	0.4
	1	5.468 40	9.262 20	2.271 33	0.4
	2–4	4.906 96	8.460 75	3.239 97	0.4

energy of the target state it leaves behind. The energy of the target state does not depend on L_c and S_c alone but on the total angular momentum of the core, J_c. To obtain the Rydberg series attached to each of the fine-structure split thresholds, we use the LS to jj frame transformation, which has been described in many other works [7,10].

If we were calculating cross sections in LS coupling, we would calculate K and d at every energy mesh point. In jj coupling we need the K and d of several LS symmetries for each total angular momentum. To avoid storing huge arrays, we calculate K and d on a coarse-energy mesh and interpolate. Actually, we do not interpolate K and d but the smoother quantities [12]:

$$\mu_{ij}=\sum_{\alpha} U_{i\alpha}\mu_{\alpha}(U^{\dagger})_{\alpha j} , \tag{5}$$

$$(d^c)_i=\sum_{j,\alpha} d_j U_{j\alpha}\cos\pi\mu_{\alpha}(U^{\dagger})_{\alpha i} , \tag{6}$$

where $\mathbf{U}_{\alpha}$ are the eigenvectors of the K matrix and the $\tan\pi\mu_{\alpha}$ are the eigenvalues of the K matrix. The coarse-energy mesh is chosen such that

$$\sum_{\alpha}|\mu_{\alpha}(\varepsilon)-\mu_{\alpha}(\varepsilon+\Delta)|<0.1 .$$

We use a linear interpolation of μ and d^c with energy between each of the coarse-energy mesh points (the possibility of μ_{α} changing branches introduces prohibitive bookkeeping for higher-order interpolation).

The physical justification for the accuracy of the frame transformation rests on a consideration of time scales. The amount of time that the electron spends interacting with the core is proportional to the derivative of the quantum defect with energy, $d\mu/dE$. The spin-orbit interaction causes the orbital angular momentum of the core to process about the direction of the total angular momentum in a time proportional to the inverse of the fine-structure energy splitting, $\Delta E_{\rm SO}$. If the time that the electron spends interacting with the core is much shorter than the precession time of the core's orbital angular momentum, one can neglect the precession during the interaction (i.e., the spin-orbit interaction can be neglected when all of the electrons are in the R-matrix box). When the electron spends a long time in the interaction region or the precession time is short ($\Delta E_{\rm SO}d\mu/dE$ is not small), the precession cannot be ignored, and therefore the spin-orbit interaction needs to be accounted for. For the heavier atoms, $\Delta E_{\rm SO}$ can be fairly large, causing a breakdown of the frame-transformation approximation. For the atoms studied in this paper, there are short-range $nsnp^3$ resonances which give large values of $d\mu/dE$ for some symmetries. These resonances cause trouble for our Ge and Sn results, which otherwise would have worked well. There is also an operational difficulty when the frame-transformation approximation breaks down. We always use the scattering parameters as a function of energy relative to the theoretical threshold. What energy does this correspond to relative to the spin-orbit split thresholds? If $\Delta E_{\rm SO}d\mu/dE$ is small, it does not matter which threshold is chosen; in general we set the theoretical threshold equal to the experiment, LS-averaged threshold. When $\Delta E_{\rm SO}d\mu/dE$ is not small (i.e., where the frame-transformation approximation breaks down), the final results are sensitive to which threshold you choose. Since there is no justification for choosing one or the other, we choose the one which gives the best agreement between theory and experiment. This is not entirely satisfactory, and it points to the need for a more sophisticated treatment than the one presented here for Ge and Sn.

TABLE II. Parameters for the semiempirical potential for the natural orbitals.

Atom	l	$\bar{\alpha}_1^l$	$\bar{\alpha}_2^l$	$\bar{\alpha}_3^l$
C	0	0.475 73	1.639 74	1.353 06
	1	0.335 98	1.430 34	1.514 74
	2–4	0.000 00	0.000 00	0.000 00
Si	0	0.294 39	2.348 99	0.930 04
	1	0.301 51	1.856 87	0.980 74
	2–4	0.000 00	0.000 00	0.000 00
Ge	0	0.280 32	2.655 35	0.903 50
	1	0.271 62	2.207 54	1.030 13
	2–4	0.000 00	0.000 00	0.000 00
Sn	0	0.213 12	3.507 38	0.781 79
	1	0.133 37	3.552 44	0.896 79
	2–4	0.000 00	0.000 00	0.000 00

B. Hartree-Fock and natural orbitals

A key requirement of any R-matrix calculation is an accurate description of the target eigenfunctions. These are the energy eigenfunctions of the residual positive ion in the energy range of interest. For the carbon-group atoms in the bound-state energy region, there is only one target state, ns^2np. However, it is necessary to use higher-energy configurations (especially of the type $nsnp^2$) to converge the K-matrix and dipole matrix elements in the bound-state region.

As described in Ref. [7], we do not use the orbitals that are eigenstates of H_V, Eq. (2), to expand the target states due to slow convergence. Instead, we use orbitals calculated using the potential

$$\bar{V}_l(r)=V_l(r)+2(1-e^{-\bar{\alpha}_1^l r})/r+|\bar{\alpha}_2^l|(1-e^{-\bar{\alpha}_3^l r})^3/r^2 . \tag{7}$$

This potential differs from that used in Ref. [7] which was identical in form to that of Eq. (2). Unlike Ref. [7], for some values of l the best convergence occurs for $\bar{V}_l(r)=V_l(r)$. The natural orbitals were constructed by superimposing the orbitals of the $\bar{V}_l(r)$ potential [13] (see Table II).

III. COMPUTATIONAL DETAILS

The atomic ground state can be represented well by a Hartree-Fock wave function of the type $ns^2np^2\,{}^3P$. However, we have used the ns and np orbitals to describe the Hartree-Fock orbitals of the ionic state which are slightly

compressed compared to the orbitals for the neutral atom. This circumstance forces us to include many basis functions which primarily represent this simple relaxation (i.e., functions like $[nsms\ ^1S]np^2$, ns^2npmp, etc.). We also include correlation effects in the ground-state basis function, which necessitates many more basis functions than for the rare-gas atoms because the ground state has nonzero spin and angular momentum.

The main effects emerge from calculations with less than ten basis functions for the ground state, but we include many more basis functions than this in order to achieve the good agreement between the cross sections calculated in the length and velocity gauges for Sn. We did not modify our choice of basis functions for the different atoms, although the radial orbitals differed from one atom to another. The ground state was composed of ~ 150 basis functions with ~ 50 different angular configurations. The most important angular configurations were ns^2np^2, ns^2npmp, $nsmsnp^2$, $nsnp^2md$, np^4, np^2md^2, and ns^2md^2. All possible angular couplings are used for each shell configuration. The disagreement between the cross sections calculated in the length and velocity gauges is typically less than 10% for all of the carbon-group atoms, which gives an indication of the convergence of both the ground-state and the final-state wave functions.

There are six different final-state LS symmetries and eight total final-state channels which enter our calculation (in what follows the target state $ns^2np\ ^2P^o$ will be shortened to $^2P^o$): $^2P^oms\ ^3P^o$, $^2P^omd\ ^3P^o$, $^2P^oms\ ^1P^o$, $^2P^omd\ ^1P^o$, $^2P^omd\ ^3D^o$, $^2P^omd\ ^1D^o$, $^2P^omd\ ^3F^o$, and $^2P^omd\ ^1F^o$. The largest basis-set sizes were ~ 275 for the $^{1,3}P^o$ symmetries. We also carried out calculations with basis sets twice as big to test convergence; the larger basis did not change our results by more than 0.03 in the quantum defects. Part of the reason for the large basis-set size was that we used the same basis (but with different orbitals) for all of the atoms.

Most of the basis functions for the final-state symmetries were not of the simple "close-coupling-channel" type (e.g., $^2P^oms\ ^3P^o$). The most important "correlation" types of basis functions had $nsnp^3$ or $nsnp^2mp$ character. This is because some of the $nsnp^3$ states fall among the $^2P^oml$ Rydberg series and interact strongly with the whole series, resulting in a strong energy dependence of the quantum-defect parameters. If the calculated $nsnp^3$ states fall at the wrong energy, the resulting Lu-Fano plots can look wildly different from the experimental ones. We constructed this part of the basis by attaching ϵp and ϵf waves to the even-parity, CI target states: $nsnp^2$, ns^2nd, and $ns^2(n+1)s$.

The complete calculation of the photoionization cross section and Lu-Fano plots for one atom including the computation of the ground-state wave function and LS to jj frame transformation required ~ 15 min of computer CPU time on a DEC station 5000/200.

IV. OSCILLATOR STRENGTHS

A. Theory

The calculation of an oscillator strength for a discrete-discrete transition from the quantum-defect parameters K_{ij} and d_i is slightly more tricky than the calculation of a photoionization cross section. This is because the final-state wave functions needed for photoionization are normalized per unit energy and are thus easy to obtain in terms of the f and g functions which are normalized per unit energy. The final-state wave function needed to calculate the oscillator strength must be normalized to unity over the infinite volume.

There are two simple ways (among many) to *derive* the normalization constant which converts wave functions of the form Eq. (3) to one which gives the oscillator strength. One way is to add to the real physical channels one unphysical open channel coupled to the physical channels. If you then formally take the limit that the coupling of the unphysical open channel to the physical closed channels goes to zero, the resulting photoionization cross section will be a Rydberg series of δ functions; the oscillator strength to each bound state can be read off from the coefficient of each δ function. A (perhaps) more straightforward method would be to use Green's theorem to obtain directly the normalization constant [9]. This can be found from

$$\int dV\ \psi_\varepsilon \psi_{\varepsilon'} = \int dV (\psi_\varepsilon H \psi_{\varepsilon'} - \psi_{\varepsilon'} H \psi_\varepsilon)/(\varepsilon' - \varepsilon)\ ,$$

with the volume being bounded by the surface $r_i = R$. The right-hand side of this equation can be expressed as a surface integral which can be evaluated analytically since the asymptotic forms of f and g are known. At the bound-state energies,

$$\psi_\varepsilon = \sum_i \psi_i A_i \rightarrow 0 \quad \text{as } r \rightarrow \infty\ . \tag{8}$$

Take the limit $\varepsilon' \rightarrow \varepsilon =$(bound-state energy); then take the limit $R \rightarrow \infty$ to obtain the normalization coefficient. Both methods give the same result (of course).

The bound states are at the energies that give $\det(K + \tan\beta) = 0$, where

$$\beta_i = \pi \nu_i = \pi / \sqrt{2(I_c - E)}\ ,$$

with I_c being the ionization threshold in atomic units. The oscillator strength to the nth bound state is

$$f_n = 2\pi(\varepsilon_n - \varepsilon_g)\left(\sum_i d_i A_i\right)^2 \times \left[3[2J_g + 1] \times \sum_{i,j} A_i A_j \frac{d}{d\varepsilon}[K_{ij} + \delta_{ij}\tan\beta_i]\right]^{-1}\Bigg|_{\varepsilon = \varepsilon_n}\ , \tag{9}$$

where all quantities are in atomic units. There is a small practical problem in numerically finding the derivative of the K-matrix elements, i.e., there are energies where K diverges. We used the derivatives of the eigenvectors and eigen quantum defects of K to obtain the derivative of K:

TABLE III. The oscillator strengths in atomic units for excitation from the C $2s^2 2p^2\,{}^3P_0$ ground state compared to those of Nussbaumer and Storey [14] and experiment [15]. The numbers in brackets denote multiplicative powers of ten.

		Oscillator strength		
Configuration	λ (Å)	Present	NS	Expt.
$2s^2 2p 3s\,{}^3P_1^o$	1656.9	1.4[−1]	1.36[−1]	1.4[−1]±15%
$2s^2 2p 3s\,{}^1P_1^o$	1613.4	8.7[−5]	5.55[−5]	
$^3P_1^o$	1328.8	5.8[−2]	4.95[−2]	6.4[−2]±13%
$2s^2 2p 4s\,{}^3P_1^o$	1280.1	6.8[−2]	2.41[−2]	2.0[−2]±20%
$^3D_1^o$	1277.2	7.3[−2]	8.90[−2]	7.4[−2]±13%
$2s^2 2p 4s\,{}^1P_1^o$	1276.5	4.2[−4]	4.50[−3]	
$^1P_1^o$	1270.1	4.6[−4]	3.88[−4]	
$^3P_1^o$	1260.7	4.2[−2]	3.66[−2]	3.6[−2]±15%

$$\frac{dK_{ij}}{d\varepsilon}=\sum_\alpha \frac{dU_{i\alpha}}{d\varepsilon}\tan(\pi\mu_\alpha)(U^\dagger)_{\alpha j} + U_{i\alpha}\tan(\pi\mu_\alpha)\frac{d(U^\dagger)_{\alpha j}}{d\varepsilon} + U_{i\alpha}\frac{d\mu_\alpha}{d\varepsilon}\frac{\pi}{\cos^2\pi\mu_\alpha}(U^\dagger)_{\alpha j}\ . \tag{10}$$

The derivatives of the eigen quantum defects and eigenvectors are obtained from derivatives of the μ matrix of Eq. (5):

$$\frac{d\mu_\alpha}{d\varepsilon}=\sum_{ij}(U^\dagger)_{\alpha j}\frac{d\mu_{ji}}{d\varepsilon}U_{i\alpha}\ , \tag{11}$$

$$\frac{dU_{i\alpha}}{d\varepsilon}=\sum_{\alpha'(\neq\alpha)}\frac{U_{i\alpha'}}{\mu_\alpha-\mu_{\alpha'}}\sum_{i,j}(U^\dagger)_{\alpha' j}\frac{d\mu_{ji}}{d\varepsilon}U_{i\alpha}\ . \tag{12}$$

We find the derivative of μ_{ij} numerically. Equations (11) and (12) avoid the problem of $\mathbf{U}_\alpha$ changing phase from one energy step to the next (among other problems).

B. Results

There are few published data on the oscillator strengths for the carbon-group atoms. Nussbaumer and Storey [14] (NS) calculated oscillator strengths for C in intermediate coupling and Goldbach *et al.* published some experimental results [15]. We compare some of their values and ours in Table III. Overall, there is good agreement between the two calculations and the experiment except for the 1280.1-Å and the 1276.5-Å lines. The 1276.5-Å line has very little oscillator strength; we do not expect good agreement for the weak transitions. The 1280.1-Å line is nearly degenerate with the 1277.2-Å line which causes $^3P_1^o$-$^3D_1^o$ mixing to depend sensitively on the spacing of these levels; the sum of the oscillator strengths for these two lines is relatively insensitive to the spacing and is equal to 0.14 (present calculation) and 0.11 (NS). Brown *et al.* [2(a)] published relative absorption strengths from the $3s^2 3p^2\,{}^3P_{J_g}$ states to states with $J=0$–3. We compare our results with theirs in Table IV for the 2→3 transition. The agreement is not very good. At energies closer to the thresholds, our results decrease much faster than those of Brown *et al.*, which do not appear to be falling like $1/n^3$.

In Figs. 1(a)–1(d) we show the oscillator strengths for transitions from the $^3P_0$ ground state. These figures are not meant to convey detailed information; they are meant to convey a feeling for the level of channel interactions for each atom. For the $J=1$ final-state symmetry, there are five channels: two Rydberg series attached to the $J_c=\frac{1}{2}$ threshold and three Rydberg series attached to the $J_c=\frac{3}{2}$ threshold. In the absence of channel interactions, the oscillator strength of each Rydberg would decrease like $(I_c-E_n)^{-3/2}$, where I_c is the energy of the ionization threshold. Channel interactions can cause the oscillator strengths to vary somewhat irregularly from level to lev-

TABLE IV. The oscillator strengths in atomic units for excitation from the Si $3s^2 3p^2\,{}^3P_2$ initial state to the $J=3$ final state compared to the relative absorption strength of Brown *et al.* [2(a)]. The numbers in brackets denote multiplicative powers of ten.

	Oscillator strength	
λ^{-1} (cm^{-1})	Present	Expt.
53 362.3	1.01[−3]	35
57 450.6	6.01[−4]	50
58 893.3	1.19[−2]	80
60 705.4	1.54[−3]	30
61 423.2	1.77[−2]	70
62 376.8	2.84[−3]	20
62 802.8	1.21[−2]	50
63 340.6	4.14[−3]	40
63 641.8	5.90[−3]	40
63 945.1	4.93[−3]	35
64 187.8	1.75[−3]	25
64 351.9	5.03[−3]	30
64 548.1[a]	9.80[−6]	
64 647.5	4.59[−3]	45[b]
64 795.4	8.95[−4]	15[b]
64 881.5	1.69[−3]	30
64 965.0	1.94[−3]	15
65 054.5[a]	1.00[−7]	
65 102.5	2.16[−3]	25
65 226.6	1.06[−4]	10

[a]Theoretical energy.
[b]Blended line.

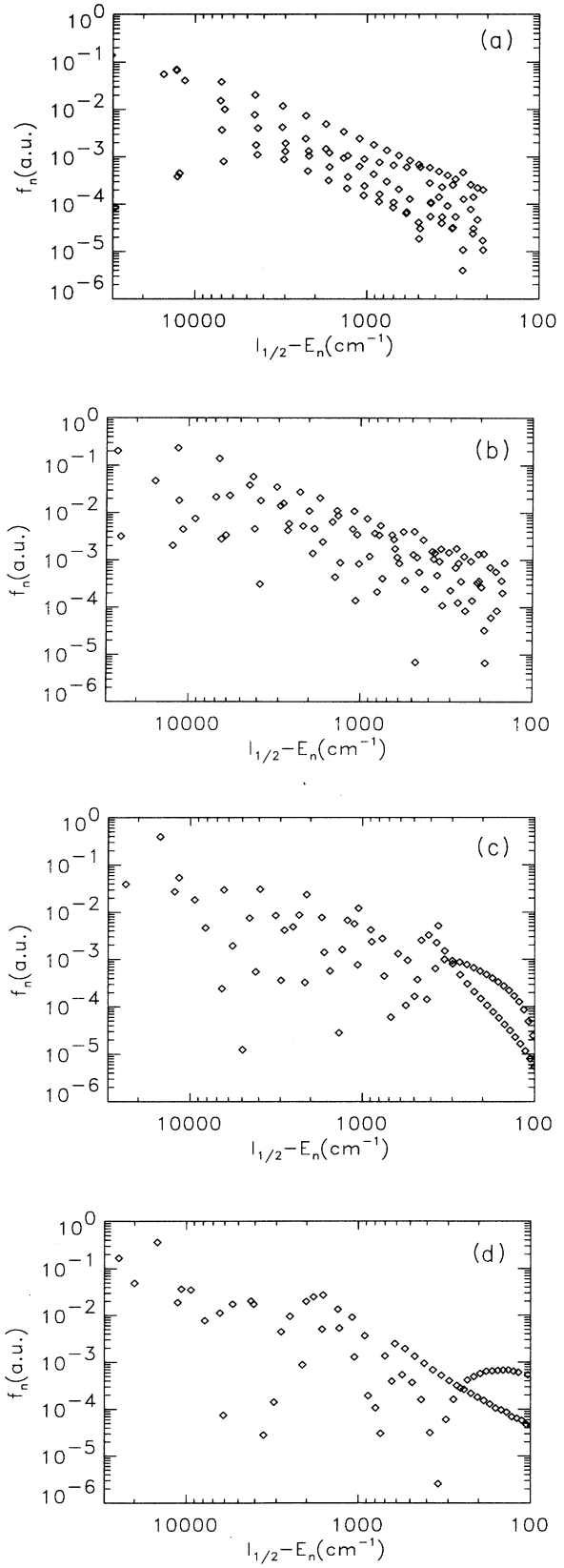

FIG. 1. Oscillator strength as a function of energy below the $J_c=\frac{1}{2}$ threshold: (a) C, (b) Si, (c) Ge, and (d) Sn.

el. However, as the energy approaches the lowest threshold, the density of states attached to that threshold diverges, while the density of states attached to the upper threshold(s) remains roughly constant; when you get close enough to the lowest threshold, the states form simple Rydberg series attached to that threshold with oscillator strengths which decrease like $(I_c-E_n)^{-3/2}$. The main part of the channel interaction is due to the frame transformation which mixes the channels of different LS symmetries; if the thresholds were not split by the spin-orbit interaction, the channel interactions would be very small.

In Fig. 1(a) we give the oscillator strengths for C whose thresholds have a spin-orbit splitting of 63 cm^{-1}. This small splitting is reflected in the appearance of *five* Rydberg series decreasing like $1/n^3$ at energies more than 1000 cm^{-1} below the $J_c=\frac{1}{2}$ threshold. At energies closer than $\sim$400 cm^{-1} to the threshold, the series have irregular strengths due to channel mixing. In this figure we do not reach the energy range where there are two simple Rydberg series attached to the $J_c=\frac{1}{2}$ threshold. In Fig. 1(b) we give the oscillator strengths for Si whose thresholds have a spin-orbit splitting of 287 cm^{-1}. This much larger splitting (than that of C) generates more channel interaction in this energy range. The oscillator strengths are correspondingly more irregular; a generic $1/n^3$ decrease is still apparent. In this figure we do not reach the energy range where there are two simple Rydberg series attached to the $J_c=\frac{1}{2}$ threshold. In Fig. 1(c) we give the oscillator strengths for Ge whose thresholds have a spin-orbit splitting of 1767 cm^{-1}. At energies more than $\sim$300 cm^{-1} below the threshold, the oscillator strengths are very irregular, indicating strong channel interactions. At energies less than $\sim$300 cm^{-1} below the threshold, we see the two simple Rydberg series attached to the $J_c=\frac{1}{2}$ threshold. These series do not have the simple $1/n^3$ dependence due to the interaction with perturbing states at $\sim$60 and at $\sim$90 cm^{-1} attached to the $J_c=\frac{3}{2}$ threshold. In Fig. 1(d) we give the oscillator strengths for Sn whose thresholds have a spin-orbit splitting of 4251 cm^{-1}. At energies more than $\sim$600 cm^{-1} below the threshold, the oscillator strengths are very irregular, indicating strong channel interactions. At energies less than $\sim$600 cm^{-1} below the threshold, we see the two simple Rydberg series attached to the $J_c=\frac{1}{2}$ threshold. One series has a simple $1/n^3$ dependence, while the other is perturbed at $\sim$320 cm^{-1} by a state attached to the $J_c=\frac{3}{2}$ threshold.

V. LU-FANO PLOTS

A Lu-Fano plot [6] provides a simple, graphical method for checking the accuracy of multichannel scattering parameters when there are only two thresholds affecting the dynamics. For each bound-state energy level, this is a plot of the pairs of points (ν_{un},ν_{ln}) where

$$\nu_{un}=[2(\varepsilon_u-\varepsilon_n)]^{-1/2}$$

and

$$\nu_{ln}=[2(\varepsilon_l-\varepsilon_n)]^{-1/2}\ (\mathrm{mod}1)\ ;$$

ε_n is the energy level in atomic units; $\varepsilon_{l(u)}$ is the lower (upper) threshold in a.u. For us, the upper threshold is $ns^2np\ ^2P_{3/2}$ and the lower threshold is $ns^2np\ ^2P_{1/2}$. We generate the theoretical results by treating the channels attached to the upper threshold as closed and those attached to the lower threshold as open in the MQDT calculation. This gives a very energy-dependent K matrix; the theoretical curves are the arctangents of the eigenvalues (divided by π) of this energy-dependent K-matrix. If the original K matrix is energy independent, the theoretical curves will be identical when $\nu_u \rightarrow \nu_u + 1$. The distance between the theoretical curves and the experimental points indicates the error in the calculation.

In Figs. 2–5 we give the Lu-Fano plots for C, Si, Ge, and Sn. The plots give the results of the present calculation as well as all of the experimental information (which we know about) for the odd-parity levels with $J=0-3$. We do not attempt to use the calculation to classify the levels because in general the states are not very pure, making classification meaningless. We clearly obtain the best agreement for all symmetries in C and Si and in the $J=0$ symmetry for Ge and Sn. The main source of the discrepancies is discussed below. In some of the Lu-Fano plots there are experimental points below the smallest value of $\nu_{3/2}$ of the theoretical curves. We did not calculate lower theoretical points because the wave functions were exponentially diverging *inside* of the R-matrix box [at negative energies the wave function of Eq. (3) always diverges], which can give spurious results after making the frame transformation. We could have obtained the Lu-Fano plots at these energies by using a smaller R-matrix box.

In Figs. 2(a)–2(d) we present the Lu-Fano plots for the odd-parity, $J=0-3$ states of C. The experimental points are taken from Ref. [1]. Carbon is qualitatively different from the heavier elements due to the very small size of its core; the maximum of the radial electron density,

$$\rho(r) \equiv \sum_i \langle \delta(r - r_i) \rangle \ ,$$

for the ns^2np ionic ground state is near 1.1 a.u. for C, 1.8 a.u. for Si, 1.8 a.u. for Ge, and 2.1 a.u. for Sn. All of the vertical and horizontal lines are within 0.1 of an integer (except at low $\nu_{3/2}$), which indicates small quantum defects for all of the LS symmetries. Above $n_{3/2} \simeq 3.5$, the pattern repeats when $\nu_{3/2} \rightarrow \nu_{3/2} + 1$, which indicates that the scattering parameters are independent of the energy in this range. The pattern below $\nu_{3/2} \simeq 3.5$ is different from that above $\nu_{3/2} \simeq 3.5$, which indicates a strong energy dependence in the scattering parameters. This energy dependence is caused by the $2s2p^3\ ^{2S+1}L$ states which appear in the calculation as resonances in the $2s^22p\ \epsilon s$ and ϵd scattering parameters. The $nsnp^3$ states give a strong energy dependence to the quantum defects over the range of the resonance. There are no $nsnp^3\ ^{1,3}F$ states; the quantum defects for the ^1F and ^3F symmetries do not have a strong energy dependence. On the whole, the theoretical curves are in good agreement with the data points; we estimate that the error in the theoretical quantum defects is less than 0.02.

In Figs. 3(a)–3(d) we present the Lu-Fano plots for the

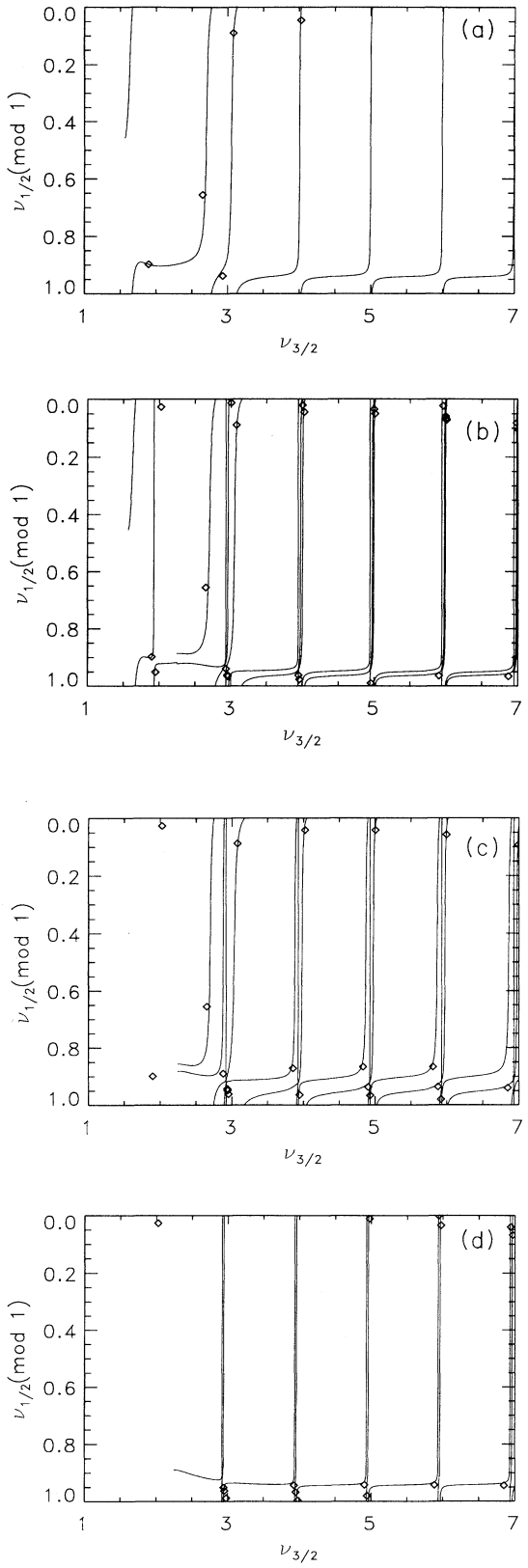

FIG. 2. Lu-Fano plots for the C odd-parity symmetries. The diamonds are the experimental points of Ref. [1]: (a) $J=0$, (b) $J=1$, (c) $J=2$, and (d) $J=3$.

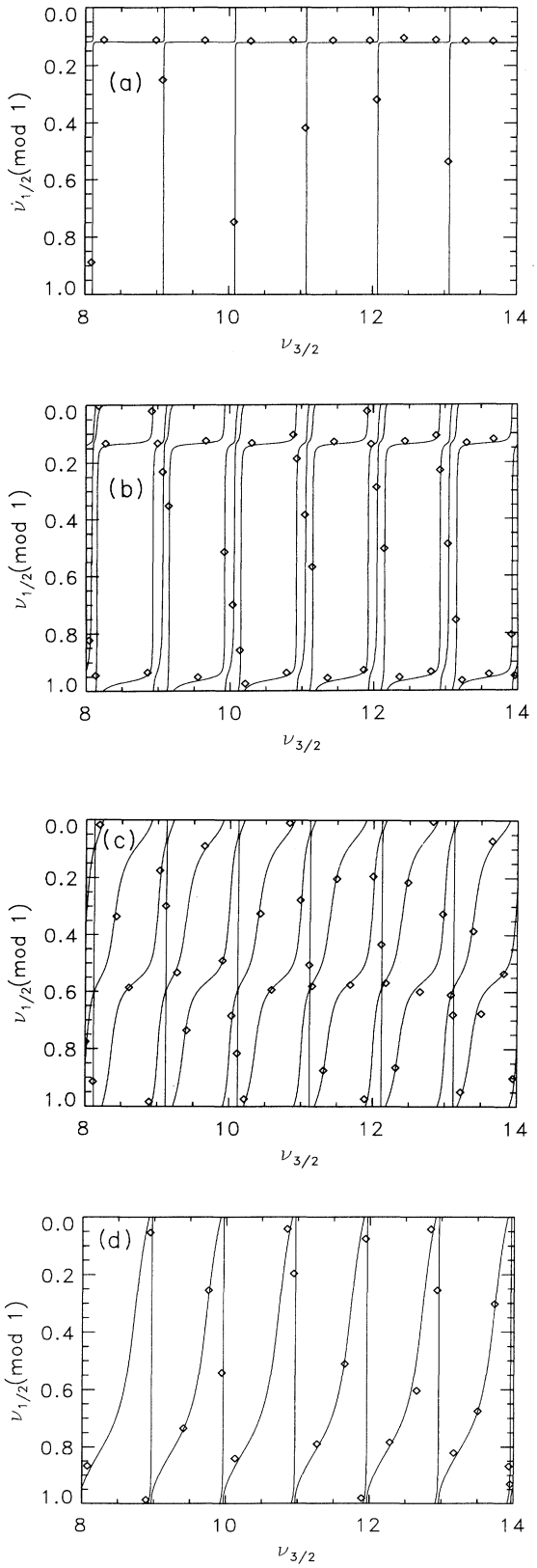

FIG. 3. Lu-Fano plots for the Si odd-parity symmetries. The diamonds are the experimental points of Refs. [2]. (a) $J=0$, (b) $J=1$, (c) $J=2$, and (d) $J=3$.

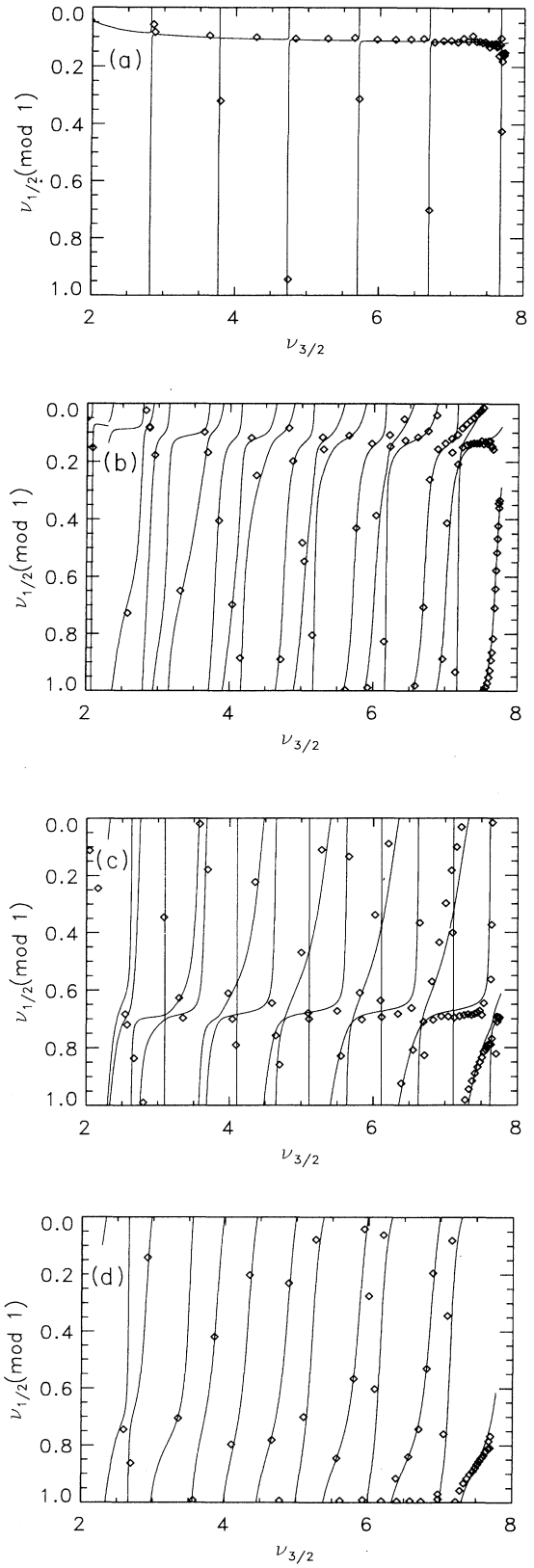

FIG. 4. Lu-Fano plots for the Ge odd-parity symmetries. The diamonds are the experimental points of Ref. [3]. (a) $J=0$, (b) $J=1$, (c) $J=2$, and (d) $J=3$.

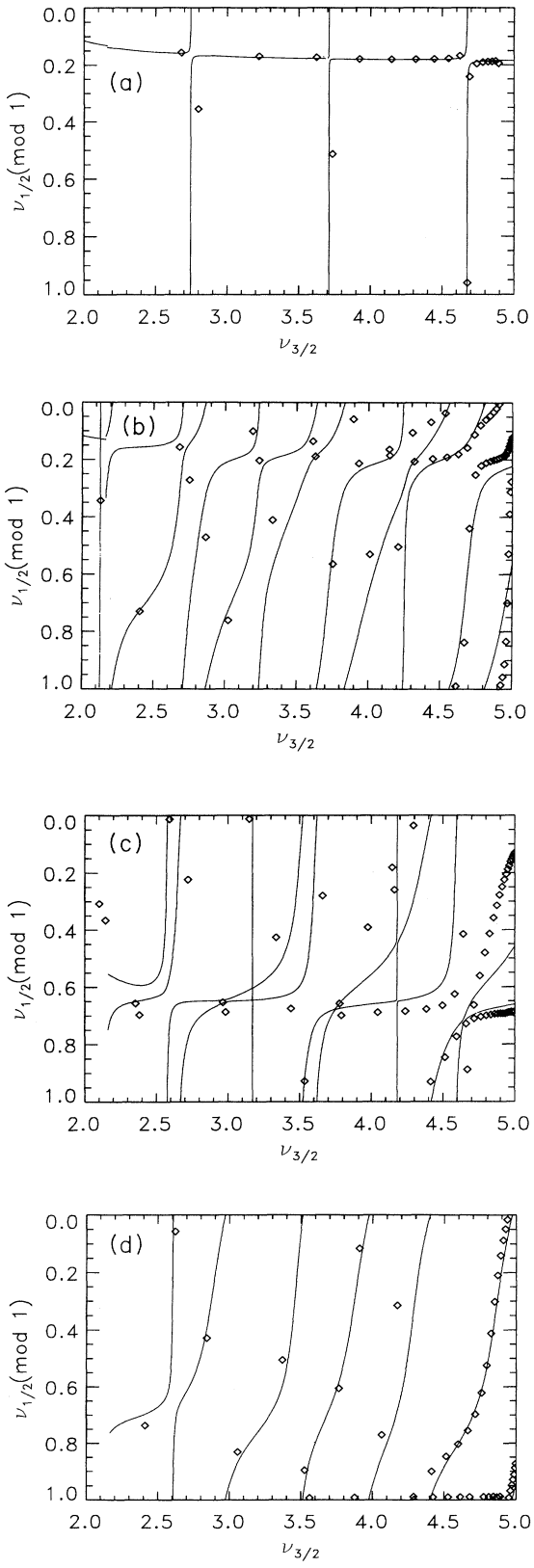

FIG. 5. Lu-Fano plots for the Sn odd-parity symmetries. The diamonds are the experimental points of Ref. [4] (a) $J=0$, (b) $J=1$, (c) $J=2$, (d) $J=3$.

odd-parity, $J=0-3$ states of Si. The experimental points are taken from Ref. [2]. Again, good agreement is found between the theoretical and experimental results; in this range we estimate that the error in the theoretical quantum defects is less than 0.02. In the energy range covered by Fig. (3), the scattering parameters are independent of the energy. At smaller values of $\nu_{3/2}$, the $3s3p^3$ states cause a large energy dependence in the scattering. For Si, Ge, and Sn, the $nsnp^3$ states cause an energy dependence over a much larger range because the $ns^2np\ \epsilon d$ can interact more strongly with these states; in C the $2s2p^3$ states are more compact than the corresponding $nsnp^3$ states of the heavier atoms and the ϵd partial wave does not penetrate as far in C as in the heavier atoms. For Si there are two curves for the $J=2$ symmetry and one curve for the $J=3$ symmetry which are very far from the lines $\nu_{1/2}=$integer or $\nu_{3/2}=$integer. These curves arise from the large phase shifts of the $3s^23p\ \epsilon d\ ^1D$ and ^3F symmetries. It is perhaps not surprising that these two symmetries have the largest quantum defects because the $1/r_{12}$ interaction between the $3p$ and ϵd electrons is the least repulsive for these symmetries.

In Figs. 4(a)–4(d) we present the Lu-Fano plots for the odd-parity, $J=0-3$ states of Ge. The experimental data points are taken from Ref. 3. The agreement between the experimental and theoretical results is not as good for Ge $J=1-3$ symmetries as it is for the two lighter atoms. The discrepancies are almost solely due to the large energy dependence of the $4s^24p\ \epsilon d\ ^3D$ quantum defect. We estimate that the quantum defects for all other symmetries have errors less than 0.03. The quantum defect for the ^3D symmetry has a large energy dependence over the whole range shown because of the large interaction with the $4s4p^3\ ^3D$ state. This large energy dependence makes the application of the LS to jj frame transformation somewhat problematical. We obtain noticeably different results when we use the energy relative to the LS-averaged threshold energy or use the energy relative to the $J_c=\frac{1}{2}$ or $\frac{3}{2}$ energies. In Fig. 6 we show the two different results when we zero the energy relative to the $J_c=\frac{1}{2}$ or $\frac{3}{2}$ thresholds; the curves which change when us-

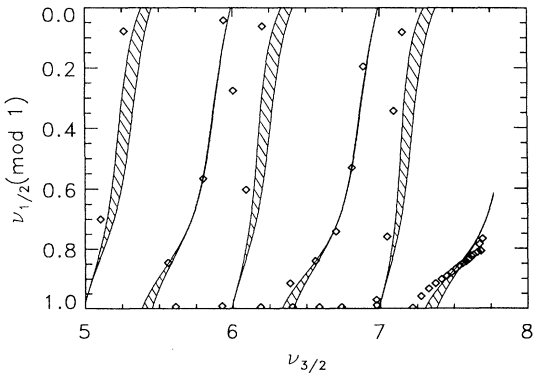

FIG. 6. Lu-Fano plots for the Ge odd-parity, $J=3$ states. The two theoretical curves are for the energy being zeroed at the $J_c=\frac{1}{2}$ and $\frac{3}{2}$ thresholds as described in the text. The region *between* the two different plots is hatched.

ing the two different scales depend on the ^3D quantum defect. In Fig. (4) we show our results when we zero to the $J_c=\frac{1}{2}$ threshold since we obtain the best match with experiment with this energy scale. The physical and technical reasons for the difficulty are discussed in Sec. II A. Carbon and Si have much smaller spin-orbit splittings and this problem does not arise for these atoms. The experimental data points near $\nu_{1/2}=1$ of Fig. 4(d) are g states; the $ns^2np\,\epsilon g$ channels were not included in the calculation.

In Figs. 5(a)–5(d) we present the Lu-Fano plots for the odd parity, $J=0-3$ states of Sn. The experimental data points are taken from Ref. [4]. The agreement between the experimental and theoretical results is not as good for the $J=1-3$ symmetries as it is for the lighter atoms. Like Ge, by far the largest error is induced by the large energy dependence of the ^3D quantum defect. Again, the quantum defect for this symmetry has a large energy dependence over the whole range shown because of the large interaction with the $5s5p^3\,^3D$ state. In Fig. 7 we show the two different results when we zero the energy relative to the $J_c=\frac{1}{2}$ and $\frac{3}{2}$ thresholds. In Fig. 5 we show our results when we zero to the $J_c=\frac{1}{2}$ threshold. The experimental data points near $\nu_{1/2}=1$ of Fig. 5(d) are g states; the $ns^2np\,\epsilon g$ channels were not included in the calculation.

Part of the reason for presenting the theoretical data for all of the atoms in one paper is to allow comparison of the same parameters for the different atoms. From Figs. 2–5 some of the basic similarities are obscured by the different ranges of $\nu_{3/2}$; to make a comparison between the different atoms, it is best to block out all but an integer range of $\nu_{3/2}$. As with the other columns of the Periodic Table, the first-row atom C is different from the heavier atoms because its d-continuum wave cannot penetrate into the core region and thus does not interact strongly with the core electrons. Previous work on other columns of the Periodic Table suggests that the heavier atoms should be very similar to each other. Although there are some striking similarities between Si, Ge, and Sn, there are also some differences. The similarities are biggest for the scattering parameters which vary the least with energy; the differences are strongest for those which vary the most with energy. This should not be surprising because the energy-dependent parameters depend on the energy relative to threshold and on the width of the perturbing $nsnp^3$ state, which can be expected to vary somewhat from atom to atom.

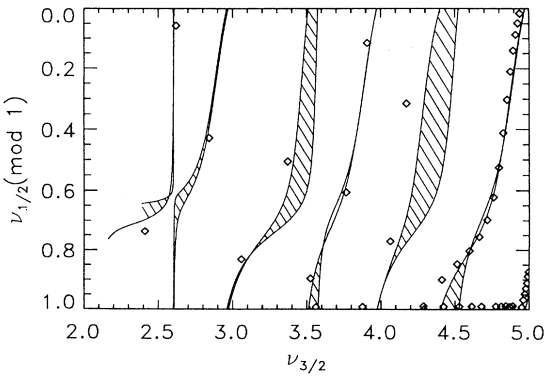

FIG. 7. Same as Fig. 6 but for Sn.

In Refs. [2(b),3,4] Brown *et al.* fitted MQDT parameters to their measured energy levels for Si ($J=2$ and 3), Ge ($J=0-3$), and Sn ($J=0-3$), assuming these parameters to be energy independent. In Ref. [5] the MQDT parameters of Si, Ge, and Sn were allowed to have energy dependence but these fits were only for $J=3$; they explicitly included the $nsnp^3\,^3D_3^o$ perturber in the MQDT parameters. Although they obtained good fits, the number of parameters needed to reach this level of agreement was much larger than the fitted parameters of Refs. [2–4]. We feel the key parameter of Ref. [5] was the larger fitted value of $d\mu/dE$ for the ^3D channel.

To obtain good agreement with experiment, it is necessary to use energy-dependent parameters. Comparisons which rest on the analysis of energy-independent parameters are suspect. A recent analysis [16] of direct s-d scattering for Si, Ge, and Sn does not give the full picture for this reason. The "size" of the s-d scattering probability can be estimated by examining the $J=0$ Lu-Fano plots; the two $J=0$ channels are $ns^2np\,^2P_{1/2}\,\epsilon s_{1/2}$ and $ns^2np\,^2P_{3/2}\,\epsilon d_{3/2}$. For zero scattering probability, the horizontal and vertical lines would cross. It can be seen in Figs. 4(a) and 5(a) that the size of the avoided crossing (and hence the s-d scattering probability) changes with energy. There are two indistinguishable paths for an s wave to scatter into a d wave: (1) the direct path, $ns^2np\,\epsilon s\rightarrow ns^2np\,\epsilon d$, and (2) the indirect path,

$$ns^2np\,\epsilon s\rightarrow nsnp^3\rightarrow ns^2np\,\epsilon d\ .$$

The amplitude for the direct path does not depend strongly on energy, while the amplitude for the indirect path does depend strongly on energy near the resonance. This shows a limitation of the Ref. [16] analysis based on empirical MQDT parameters from Refs. [2–4], as we find that it is impossible to extract a direct s-d scattering probability that is roughly independent of energy.

We do not give tables of our MQDT parameters because of their large energy dependence. The tables would need to be either large or else relevant to only a small energy range.

VI. AUTOIONIZATION SPECTRA

In Figs. 8(a)–8(d) we present the photoionization cross section as a function of $\nu_{3/2}$ for the different atoms for excitation from the $ns^2np^2\,^3P_0$ ground state. For the $J=1$ final state, there are three Rydberg series attached to the $J_c=\frac{3}{2}$ threshold which can be clearly seen in Fig. 8 except for C, Fig. 8(a), where the two d-wave resonances cannot be distinguished. Classifying the resonances is somewhat meaningless due to channel interactions. However, the s-d mixing is comparatively weak, so we can identify the s-wave resonances as the very sharp resonances in C at $\nu_{3/2}\simeq n+0.94$, the resonances in Si at $\nu_{3/2}\simeq n+0.15$, the sharp resonances in Ge at $\nu_{3/2}\simeq n+0.18$, and the sharp resonances in Sn at

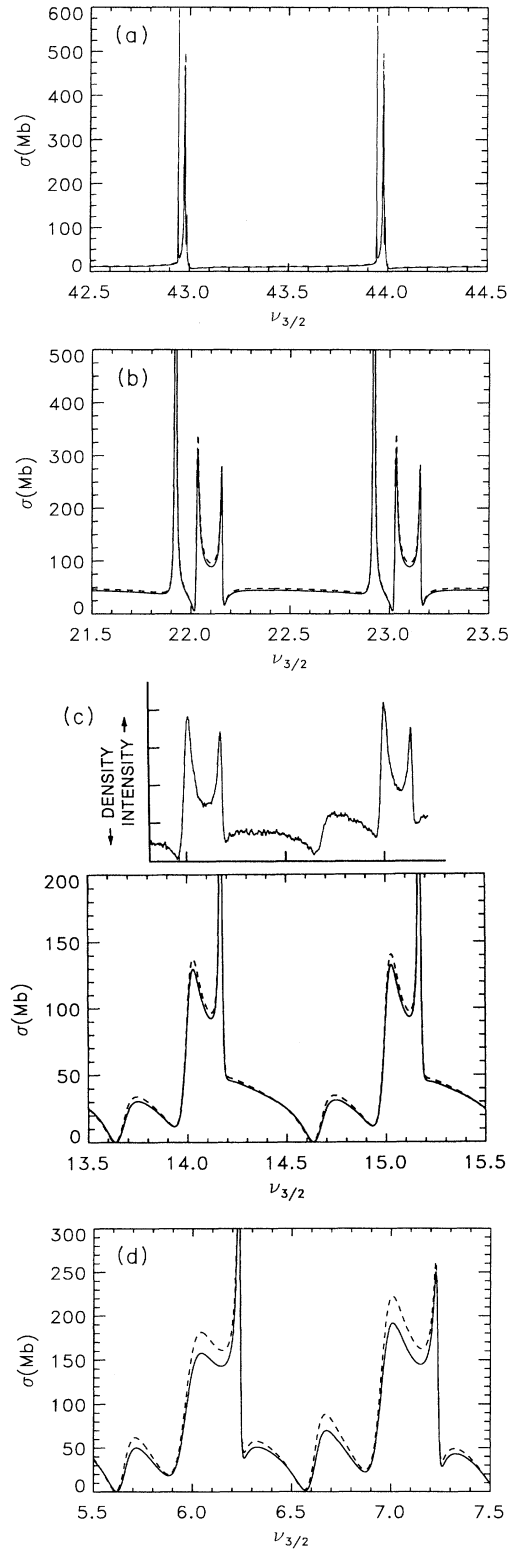

FIG. 8. The photoionization cross section calculated in length (dashed line) and velocity (solid line) gauges between the $J_c=\frac{1}{2}$ and $\frac{3}{2}$ thresholds: (a) C, (b) Si (the height of the s-wave resonance is $\sim$1300 Mb), (c) Ge with the densitometer trace of Ref. [3] (the height of the s-wave resonance is $\sim$750 Mb), and (d) Sn.

$\nu_{3/2}\simeq n+0.21$. The two d-wave resonances are at $\nu_{3/2}\simeq n+0.98$ and $\nu_{3/2}\simeq n+0.99$ in C, at $\nu_{3/2}\simeq n+0.92$ and $\nu_{3/2}\simeq n+0.03$ in Si, at $\nu_{3/2}\simeq n$ and $\nu_{3/2}\simeq n+0.75$ in Ge, and at $\nu_{3/2}\simeq n$ and $\nu_{3/2}\simeq n+0.7$ in Su. If the scattering parameters were energy independent, the autoionization cross section would repeat at $\nu_{3/2}\rightarrow\nu_{3/2}+1$. It is clear for Sn that the pattern does not repeat in going from $\nu_{3/2}\simeq 6$ to $\nu_{3/2}\simeq 7$ which is a change in energy of $\sim$0.004 a.u. (compare to the spin-orbit splitting of $\sim$0.02 a.u. for Sn^+). The Ge cross section repeats when going from $\nu_{3/2}\simeq 14$ to $\nu_{3/2}\simeq 15$, which is a very small energy change; however, when we compare the autoionization cross section near $\nu_{3/2}\simeq 8.5$ to that near $\nu_{3/2}\simeq 25.5$, we see a noticeable difference.

The only experimental data which we know of in this energy range is the densitometer trace of Brown, Tilford, and Ginter [3], Fig. 11. We give their results above ours in Fig. 8(c). Our cross section is similar to theirs with the exception of the height and q value of the s-wave resonance at $\nu_{3/2}\simeq n+0.18$. The positions of the resonances are in pretty good agreement. Resonance shapes are more difficult to reproduce; our problems with the frame transformation discussed above might account for the discrepancies. Alternatively, it should be kept in mind that densitometer traces are not linear in intensity, and accordingly may distort line-shape profiles.

The small widths of the C autoionizing resonances compared to the heavier atoms should not be surprising because the C d waves do not interact strongly with the core. The autoionizing spectra for the heavier atoms do not resemble each other as closely as might be expected; the Si spectrum in particular looks very different from the Ge and Sn spectra. This is again due to the large energy dependence in some of the scattering parameters caused by $nsnp^3$ perturbers.

VII. CONCLUSIONS

In this paper we have compared our calculated scattering parameters to those of previous experiments through the use of Lu-Fano plots as well as by direct comparison to experimental and calculated oscillator strengths for a couple of C transitions. The calculations show good agreement with experiment for C and Si and for the $J=0$ symmetry of Ge and Sn.

The main reason for discrepancies is the rapid energy dependence of the $^3D^o$ quantum defect near threshold. This energy dependence causes problems in the implementation of the LS to jj frame transformation for the $J=1-3$ symmetries. A large energy dependence of a quantum defect implies that the electron spends a long time in the interaction region in that channel; the frame transformation assumes that the time the electron spends interacting with the core is *short* compared to the spin-orbit precession time. The $nsnp^3$ short-range states cause energy dependences in the $^{1,3}P^o$ and $^{1,3}D^o$ symmetries with the strongest effect near threshold in the $^3D^o$ symmetry. Any *detailed* information which rests on the assumption of energy-independent MQDT reaction matrices should be viewed as suspect.

These calculations emphasize the need for accurate

energy-level data for alkalilike ions throughout the Periodic Table. By incorporating such data into a semiempirical model potential, the main polarization and screening effects of inner-shell core electrons can be built into the calculation efficiently at the start. Both Ref. [7] and the present calculations have suffered from the limited amount of ionic level information that is available, especially for the heavier alkalilike ions.

Of particular interest is the degree of similarity between the different atoms. However, the similarities do not appear to be as striking as those within other atomic groups, like the rare-gas atoms or the halogens. This is partly due to the nature of Lu-Fano plots, which depend sensitively on the quantum defects. Most of the differences between the atoms are in the symmetries with the most energy dependence; the slight differences in energies relative to threshold and in the widths of the $nsnp^3$ resonances for the different atoms can translate into large differences in quantum defects. Those parameters with small energy dependences are similar in Si, Ge, and Sn; this similarity is hard to see in the Lu-Fano plots because the frame transformation mixes several LS symmetries (except for the $J=0$ symmetry).

ACKNOWLEDGMENTS

This research is supported by the Division of Chemical Sciences, Office of Basic Energy Sciences, Office of Energy Research, U. S. Department of Energy, Grant No. DE-FG-02-90ER14145.

[1] C. E. Moore, *Atomic Energy Levels,* Natl. Bur. Stand. (U.S.) Circ. No. 467 (U.S. GPO, Washington, DC, 1949), Vol. I; U. Feldman, C. M. Brown, G. A. Doschek, C. E. Moore, and F. D. Rosenberg, J. Opt. Soc. Am. **66**, 853 (1976).

[2] (a) C. M. Brown, S. G. Tilford, R. Tousey, and M. L. Ginter, J. Opt. Soc. Am. **64**, 1665 (1974); (b) C. M. Brown and S. G. Tilford, *ibid.* **65**, 385 (1975).

[3] C. M. Brown, S. G. Tilford, and M. L. Ginter, J. Opt. Soc. Am. **67**, 584 (1977).

[4] C. M. Brown, S. G. Tilford, and M. L. Ginter, J. Opt. Soc. Am. **67**, 607 (1977).

[5] D. S. Ginter, M. L. Ginter, and C. M. Brown, J. Chem. Phys. **85**, 6530 (1986); D. S. Ginter and M. L. Ginter, *ibid.* **85**, 6536 (1986).

[6] K. T. Lu and U. Fano, Phys. Rev. A **2**, 81 (1970).

[7] (a) F. Robicheaux, and C. H. Greene, Phys. Rev. A **46**, 3821 (1992); (b) **47**, 1066 (1993).

[8] C. H. Greene and L. Kim, Phys. Rev. A **38**, 5953 (1988); C. H. Greene and M. Aymar, *ibid.* **44**, 1773 (1991), and references therein.

[9] U. Fano and A. R. P. Rau, *Atomic Collisions and Spectra* (Academic, Orlando, 1986); M. J. Seaton, Rep. Prog. Phys. **46**, 167 (1983).

[10] C. M. Lee and K. T. Lu, Phys. Rev. A **8**, 1241 (1973).

[11] W. Johnson, D. Kolb, and K. -N. Huang, At. Data Nucl. Data Tables **28**, 333 (1983).

[12] C. H. Greene and Longhuan Kim, Phys. Rev. A **36**, 2706 (1987).

[13] P. O. Löwdin, Phys. Rev. **97**, 1474 (1955); P. O. Löwdin and H. Shull, *ibid.* **101**, 1730 (1956); C. Froese-Fischer, J. Comput. Phys. **13**, 502 (1973).

[14] H. Nussbaumer and P. J. Storey, Astron. Astrophys. **140**, 383 (1984).

[15] C. Goldbach and G. Nollez, Astron. Astrophys. **181**, 203 (1987); C. Goldbach, M. Martin, and G. Nollez, *ibid.* **221**, 155 (1989).

[16] C. H. Greene, J. Opt. Soc. Am. B **4**, 775 (1987).